INTERNATIONAL JOURNAL FOR NUMERICAL METHODS IN FLUIDS
Int. J. Numer. Meth. Fluids 2003; **43**:147–163 (DOI: 10.1002/fld.601)

A fully implicit method for steady and unsteady viscous flow simulations

Jie Li*,†, Fengwei Li‡ and Qin E

Department of Aircraft Engineering, Northwestern Polytechnical University, P.O. Box 114, Xi'an, Shaanxi, 710072, People's Republic of China

SUMMARY

In this paper a time-accurate, fully implicit method has been applied to solve a variety of steady and unsteady viscous flow problems. It uses a finite volume cell-centred formulation on structured grids and employs central space discretization with artificial dissipation for the residual computation. In order to obtain a second-order time-accurate implicit scheme, a Newton-like subiteration is performed in the original LU-SGS method to converge the calculations at each physical time step by means of a dual-time approach proposed by Jameson. The numerical experiments show that the present method is very efficient, reliable, and robust for steady and unsteady viscous flow simulations, especially for some low speed flow problems. Copyright © 2003 John Wiley & Sons, Ltd.

KEY WORDS: Navier–Stokes equations; fully implicit scheme; Newton subiteration

1. INTRODUCTION

One of the most important objectives of computational fluid dynamics (CFD) is to obtain the reliable numerical data for aerodynamic design of new aircraft. Navier–Stokes flow solver is necessary for this purpose.

During the past two decades, a range of methods has been developed for solving the Navier–Stokes equations [1–13]. Among them, explicit methods such as multi-stage Runge–Kutta schemes are popular for steady-state calculations [1–6]. In general, acceleration techniques such as local time stepping and implicit residual smoothing have been employed to speed up convergence in explicit ones. According to authors' computing experience, however, the convergence rate of some explicit codes well developed towards the transonic flows always slows down dramatically for some low speed flow problems, even resulting in inaccurate solutions. We think that the reason is likely to be the employment of local time-stepping technique.

*Correspondence to: Jie Li, Institute of Fluid Mechanics, Department of Aircraft Engineering, Northwestern Polytechnical University, No. 127, Youyi Xi Road, Xi'an, Shaanxi, 710072, People's Republic of China.
†E-mail: lijieruihao@163.com
‡E-mail: fwli@nwpu.edu.cn

Received 9 November 2002
Revised 4 May 2003

In this way, an implicit time-marching method is usually required to improve the convergence in the flow field computation. This requirement is particularly true for low speed and high Mach number flows where the practical stability limit of explicit methods is particularly severe.

On the other hand, it is yet desirable to develop an implicit scheme for unsteady flow simulations, where the time step is solely determined by the flow physics and is not limited by numerical stability consideration.

Relating to the construction of any numerical scheme, accuracy must be a primary consideration. Another important issue is the efficiency and robustness of the numerical method, this is especially important for computing unsteady flows where a large number of time steps may be required.

Many implicit schemes have been developed and applied successfully to steady and unsteady flow simulations [7–17]. In Reference [10], Yoon and Jameson devised an efficient implicit LU-SGS scheme by combining the LU factorization with a symmetric Gauss–Seidel relaxation technique. Following this method, the LU factors are carefully constructed in such a way to make the L and U operators scalar diagonal matrices, and it requires only scalar diagonal inversions. Due to its high efficiency, the LU-SGS method has become increasingly popular, and many improvements to this technique have been proposed in recent years.

Whereas the LU-SGS scheme is unconditionally stable and fast, it is limited to first-order accuracy in time. With the original LU-SGS scheme, a special first-order approximation is usually employed in linearizing the left-hand side resulting in the reduction of the block diagonal matrices to diagonal matrices. As a result, the LU-SGS scheme is free from any matrix inversion. All of the off-diagonal matrices contribute to the implicit operator through one forward and one backward sweep of a Gauss–Seidel iteration, thus drastically improving efficiency over an explicit scheme. Moreover, an explicit treatment is usually applied to the linearization of the viscous fluxes. These special treatments used in deriving LU-SGS do degrade convergence rate, especially after several orders of convergence.

To tackle such problem, the ideas put forward by Jameson [17] are used for reference in this paper as pseudo-time to develop a second-order time-accurate, fully implicit method by reducing the factorization and linearization errors. Follows Jameson, a Newton-like subiteration is performed to converge the calculations at each physical time step before progressing the solution to the next time step.

The present method is applied to compute a variety of steady and unsteady viscous flow problems. The numerical results show that the method is very efficient, reliable, and robust for steady and unsteady viscous flow simulations.

2. GOVERNING EQUATIONS AND ITS SEMI-DISCRETE FINITE VOLUME FORM

The unsteady compressible Navier–Stokes equations for a moving rigid control volume can be expressed in integral form as

$$\frac{\partial}{\partial t}\int_{V(t)} \mathbf{U}\,\mathrm{d}V + \int_{S(t)} \mathbf{F}\cdot\mathbf{n}\,\mathrm{d}S = \frac{1}{Re}\int_{S(t)} \mathbf{F}_{\mathrm{v}}\cdot\mathbf{n}\,\mathrm{d}S \tag{1}$$

where $V(t)$ is the moving control volume, $S(t)$ its boundary, $\mathbf{n}$ the unit outward normal vector to the boundary.

Let $\mathbf{q}_b$ denote the velocity of the moving boundary, then the convective flux can be expressed as $\mathbf{F} = \mathbf{F}_i - \mathbf{U}\mathbf{q}_b$. Here the variables $\mathbf{U}$, $\mathbf{F}_i$ and $\mathbf{F}_v$ represent, respectively, the flow variable vector, the corresponding inviscid and viscous flux terms.

The equation of state for the perfect gas

$$P = (\gamma - 1)\rho\{E - 0.5(u^2 + v^2 + w^2)\}$$

completes the governing equations. The Baldwin–Lomax turbulence model is used for turbulence closure [18]. In the current work, a thin-layer approximation is used.

The governing equation (1) is discretized using a finite volume cell-centred scheme, where the cell-averaged variables are stored at the cell centres of the grid. This permits the simulation of realistic problems by allowing the use of arbitrary structured grid.

This finite volume approximation yields the following semi-discrete system of non-linear equations for a given grid cell

$$\frac{\partial}{\partial t}(V_{i,j,k}\mathbf{U}_{i,j,k}) + \mathbf{Q}_{i,j,k} = \frac{1}{Re}\mathbf{Q}^{v}_{i,j,k} \tag{2}$$

where $\mathbf{Q}_{i,j,k}$ and $\mathbf{Q}^{v}_{i,j,k}$ are, respectively, the net convective and viscous flux out of the cell.

3. LU-SGS IMPLICIT SCHEME WITH DUAL-TIME-STEPPING TECHNIQUE

To achieve a high numerical efficiency, an explicit treatment is usually applied to the linearization of the viscous fluxes, that is, the viscous terms are time lagged. For unsteady flow calculation, the explicit treatment of the viscous terms, the approximation of the flux Jacobian matrices and the linearization procedure in the original LU-SGS method reduce the accuracy of the time discretization. To overcome this difficulty a Newton-like subiteration is introduced through a pseudo-time τ to write the problem of solving for the pseudo steady state as

$$\frac{\partial}{\partial \tau}(V_{i,j,k}\mathbf{U}_{i,j,k}) + V_{i,j,k}\frac{3\mathbf{U}^{n+1}_{i,j,k} - 4\mathbf{U}^{n}_{i,j,k} + \mathbf{U}^{n-1}_{i,j,k}}{2\Delta t} + \mathbf{Q}^{n+1}_{i,j,k} = \frac{1}{Re}\,\mathbf{Q}^{v}_{i,j,k}{}^{n} \tag{3}$$

This corresponds to add a pseudo-time derivative of dependent variable vector to Equation (1), which may be written as

$$\frac{\partial}{\partial \tau}\int_{V(t)} \mathbf{U}\,\mathrm{d}V + \frac{\partial}{\partial t}\int_{V(t)} \mathbf{U}\,\mathrm{d}V + \int_{S(t)} \mathbf{F}\cdot\mathbf{n}\,\mathrm{d}S = \frac{1}{Re}\int_{S(t)} \mathbf{F}_v\cdot\mathbf{n}\,\mathrm{d}S \tag{4}$$

Using a backward first-order accuracy time-difference formula to discretize the pseudo-time derivative Equation (3) becomes

$$V_{i,j,k}\frac{\mathbf{U}^{m+1}_{i,j,k} - \mathbf{U}^{m}_{i,j,k}}{\Delta\tau} + V_{i,j,k}\frac{3\mathbf{U}^{m+1}_{i,j,k} - 4\mathbf{U}^{n}_{i,j,k} + \mathbf{U}^{n-1}_{i,j,k}}{2\Delta t} + \mathbf{Q}^{m+1}_{i,j,k} = \frac{1}{Re}\mathbf{Q}^{v}_{i,j,k}{}^{m} \tag{5}$$

where m denotes the pseudo-time. It should be noticed that the idea of using subiterations is to converge the solution at each physical time step. Equation (5) can be rewritten as follows:

$$V_{i,j,k}\frac{\mathbf{U}^{m+1}_{i,j,k} - \mathbf{U}^{m}_{i,j,k}}{\Delta\tau} + V_{i,j,k}\frac{3(\mathbf{U}^{m+1}_{i,j,k} - \mathbf{U}^{m}_{i,j,k}) + 3\mathbf{U}^{m}_{i,j,k} - 4\mathbf{U}^{n}_{i,j,k} + \mathbf{U}^{n-1}_{i,j,k}}{2\Delta t} + \mathbf{Q}^{m+1}_{i,j,k} = \frac{1}{Re}\,\mathbf{Q}^{v}_{i,j,k}{}^{m} \tag{6}$$

Let A, B, and C be the Jacobian matrices of the convective normal flux components at the cell interfaces along the i, j, and k-directions, respectively. The convective flux $\mathbf{Q}_{i,j,k}^{m+1}$ can then be linearized about the time level m. After dropping terms of the second and higher order, this yields:

$$\begin{aligned}\mathbf{Q}_{i,j,k}^{m+1} &= \mathbf{Q}_{i,j,k}^{m} + (A\Delta\mathbf{U})_{i+1/2,j,k}^{m} - (A\Delta\mathbf{U})_{i-1/2,j,k}^{m} \\ &\quad + (B\Delta\mathbf{U})_{i,j+1/2,k}^{m} - (B\Delta\mathbf{U})_{i,j-1/2,k}^{m} + (C\Delta\mathbf{U})_{i,j,k+1/2}^{m} - (C\Delta\mathbf{U})_{i,j,k-1/2}^{m} \end{aligned} \tag{7}$$

Then the discrete equation can be expressed in the following delta form:

$$\begin{aligned}&\left[\left(\frac{V_{i,j,k}}{\Delta\tau} + \frac{3}{2}\frac{V_{i,j,k}}{\Delta t}\right) I + \delta_\xi A + \delta_\eta B + \delta_\zeta C\right]\Delta\mathbf{U}^m \\ &\quad = -V_{i,j,k}\frac{3\mathbf{U}_{i,j,k}^{m} - 4\mathbf{U}_{i,j,k}^{n} + \mathbf{U}_{i,j,k}^{n-1}}{2\Delta t} - \left(\mathbf{Q}_{i,j,k}^{m} - \frac{1}{Re}\mathbf{Q}_{i,j,k}^{\mathrm{v}\,m}\right)\end{aligned} \tag{8}$$

where $\Delta\mathbf{U}^m = \mathbf{U}_{i,j,k}^{m+1} - \mathbf{U}_{i,j,k}^{m}$. And δ_ξ, δ_η, δ_ζ denote the spatial operators along the i,j,k-directions, respectively.

Setting $\Delta\tau \to \infty$ yields a Newton-like subiteration to the pseudo-time system. The above scheme becomes

$$\left[\frac{3}{2}I + \alpha(\delta_\xi A + \delta_\eta B + \delta_\zeta C)\right]\Delta\mathbf{U}^m = -\frac{3\mathbf{U}_{i,j,k}^{m} - 4\mathbf{U}_{i,j,k}^{n} + \mathbf{U}_{i,j,k}^{n-1}}{2} - \Delta t\,\boldsymbol{R}_{i,j,k}^{m} \tag{9}$$

where $\alpha = \Delta t/V_{i,j,k}$, $\boldsymbol{R}_{i,j,k}^{m} = 1/V_{i,j,k}(\mathbf{Q}_{i,j,k}^{m} - 1/Re\,\mathbf{Q}_{i,j,k}^{\mathrm{v}\,m})$ is the flux residual vector for the grid cell (i,j,k).

Referencing to the ideas of Yoon and Jameson, the implicit LU operator can be obtained as follows.

First, using flux difference concepts, the contribution of the convective flux Jacobians at each cell face is split into the positive and negative part.

$$\begin{aligned}(A\Delta\mathbf{U})_{i+1/2,j,k} &= A_{i,j,k}^{+}\Delta\mathbf{U}_{i,j,k} + A_{i+1,j,k}^{-}\Delta\mathbf{U}_{1+i,j,k} \\ (A\Delta\mathbf{U})_{i-1/2,j,k} &= A_{i-1,j,k}^{+}\Delta\mathbf{U}_{i-1,j,k} + A_{i,j,k}^{-}\Delta\mathbf{U}_{i,j,k} \\ (B\Delta\mathbf{U})_{i,j+1/2,k} &= B_{i,j,k}^{+}\Delta\mathbf{U}_{i,j,k} + B_{i,j+1,k}^{-}\Delta\mathbf{U}_{i,j+1,k} \\ (B\Delta\mathbf{U})_{i,j-1/2,k} &= B_{i,j-1,k}^{+}\Delta\mathbf{U}_{i,j-1,k} + B_{i,j,k}^{-}\Delta\mathbf{U}_{i,j,k} \\ (C\Delta\mathbf{U})_{i,j,k+1/2} &= C_{i,j,k}^{+}\Delta\mathbf{U}_{i,j,k} + C_{i,j,k+1}^{-}\Delta\mathbf{U}_{i,j,k+1} \\ (C\Delta\mathbf{U})_{i,j,k-1/2} &= C_{i,j,k-1}^{+}\Delta\mathbf{U}_{i,j,k-1} + C_{i,j,k}^{-}\Delta\mathbf{U}_{i,j,k}\end{aligned}$$

The flux Jacobian matrices $A^{\pm}$, $B^{\pm}$, and $C^{\pm}$ are constructed so that the eigenvalues of $(^{+})$ matrices are non-negative and those of $(^{-})$ matrices are non-positive. The development of these matrices is extremely important for the success of LU-type scheme. In order to ensure

a greater diagonal dominance of the LU factors for a well-conditioned implicit algorithm, the splitting proposed by Yoon and Jameson is used in the present work.

The Jacobian matrix $A = A^+ + A^-$ is approximated by

$$A^{\pm} = \frac{A \pm r_A}{2} \tag{10}$$

where

$$r_A = \mathrm{Max}(|\lambda_A|)$$

and λ_A is the eigenvalue of Jacobian matrix A. A similar procedure is applied to the Jacobian matrices B and C.

With these approximations the dual-time-stepping scheme may be written as follows:

$$(L + D)D^{-1}(D + U)\Delta \mathbf{U}^m = -\frac{3\mathbf{U}^m_{i,j,k} - 4\mathbf{U}^n_{i,j,k} + \mathbf{U}^{n-1}_{i,j,k}}{2} - \Delta t \boldsymbol{R}^m_{i,j,k} \tag{11}$$

where

$$L = -\alpha(A^+_{i-1,j,k} + B^+_{i,j-1,k} + C^+_{i,j,k-1})$$

$$D = [3/2 + \alpha(r_A + r_B + r_C)]I$$

$$U = \alpha(A^-_{i+1,j,k} + B^-_{i,j+1,k} + C^-_{i,j,k+1})$$

The initial values for the subiteration are taken as $\mathbf{U}^m_{i,j,k} = \mathbf{U}^n_{i,j,k}$. Starting with $m = 1, \mathbf{U}^1_{i,j,k} = \mathbf{U}^n_{i,j,k}$, the sequence of iterations $\mathbf{U}^m_{i,j,k}$, $m = 1, 2, 3, \ldots$ converges to $\mathbf{U}^{n+1}_{i,j,k}$, when the right-hand side unsteady residual equals to zero.

At convergence of the pseudo-time iterations $\Delta \mathbf{U}^m \to 0$, the accuracy of the solution at each physical time step is the accuracy of the discretized unsteady governing equations. That is to say, in the case of convergence, $\mathbf{U}^{m+1}_{i,j,k} \to \mathbf{U}^{n+1}_{i,j,k}$ and $\boldsymbol{R}^m_{i,j,k} \to \boldsymbol{R}^{n+1}_{i,j,k}$, then the following equation is valid:

$$\frac{3\mathbf{U}^{n+1}_{i,j,k} - 4\mathbf{U}^n_{i,j,k} + \mathbf{U}^{n-1}_{i,j,k}}{2} + \Delta t\, \boldsymbol{R}^{n+1}_{i,j,k} = 0 \tag{12}$$

Substituting $\boldsymbol{R}^{n+1}_{i,j,k} = 1/V_{i,j,k}(\mathbf{Q}^{n+1}_{i,j,k} - 1/Re\, \mathbf{Q}^{\mathrm{v}}{}^{n+1}_{i,j,k})$ into the above equation yields a fully second-order implicit scheme in time for the governing equation,

$$V_{i,j,k}\frac{3\mathbf{U}^{n+1}_{i,j,k} - 4\mathbf{U}^n_{i,j,k} + \mathbf{U}^{n-1}_{i,j,k}}{2\Delta t} + \mathbf{Q}^{n+1}_{i,j,k} = \frac{1}{Re}\mathbf{Q}^{\mathrm{v}}{}^{n+1}_{i,j,k} \tag{13}$$

Note that in this case the viscous terms are no longer time lagged. Through the subiterations in the pseudo-time, the linearization and factorization errors go to zero, and the full temporal accuracy of the numerical discretization is recovered.

The computing practices show that the rate of convergence with the pseudo-time level is very fast, and only a few subiterations are needed.

4. CALCULATING OF FLUX RESIDUAL AND ARTIFICIAL DISSIPATION MODEL

In the present paper, the flux residual term is defined as

$$\boldsymbol{R} = \frac{1}{V}\left(\mathbf{Q} - \frac{1}{Re}\mathbf{Q}^{\mathrm{v}}\right) \tag{14}$$

All spatial derivatives appearing in $\boldsymbol{R}$ are differenced using second-order accurate central differences for the calculating of the flux residual. That is, the convective and diffusive fluxes on each cell face are calculated after computing the necessary flow quantities at the face centre. Those quantities are obtained by a simple averaging of adjacent cell-centre values of the dependent variables.

As suggested by Jameson, a blend of second and fourth order non-linear dissipation is used to avoid spurious oscillations in the vicinity of shocks and to stabilize the scheme. After introducing the artificial dissipation, the residual term becomes

$$\boldsymbol{R} = \frac{1}{V}\left(\mathbf{Q} - \frac{1}{Re}\mathbf{Q}^{\mathrm{v}} - \mathbf{D}\right) \tag{15}$$

The artificial dissipative term $\mathbf{D}$ is defined as

$$\mathbf{D} = (D_i^2 + D_j^2 + D_k^2 - D_i^4 - D_j^4 - D_k^4)\mathbf{U}_{i,j,k} \tag{16}$$

The second and fourth difference operates read [19, 20]

$$D_i^2\mathbf{U}_{i,j,k} = \nabla_i\left[\frac{1}{2}(f_{i,j,k}r_{i,j,k} + f_{i+1,j,k}r_{i+1,j,k})\varepsilon^{(2i)}\right]\Delta_i\mathbf{U}_{i,j,k}$$

$$D_i^4\mathbf{U}_{i,j,k} = \nabla_i\left[\frac{1}{2}(f_{i,j,k}r_{i,j,k} + f_{i+1,j,k}r_{i+1,j,k})\varepsilon^{(4i)}\right]\Delta_i\nabla_i\Delta_i\mathbf{U}_{i,j,k}$$

and

$$f_{i,j,k} = \min\left[1.0, 0.1 + 0.9\left(\frac{u^2 + v^2 + w^2}{M_\infty^2}\right)\right]$$

where Δ_i and ∇_i are forward and backward difference operators in the i direction.

The parameter f is introduced to reduce the artificial dissipation in the boundary layer in order not to dominate over the physical dissipation. In order to avoid excessively large dissipation level for cells with high aspect ratios and to maintain the good damping properties of the scheme, a variable scaling factor of the dissipative term [20] is employed,

$$r_{i,j,k} = (\varphi_\xi)_{i,j,k}(r_\xi)_{i,j,k}$$

$$(\varphi_\xi)_{i,j,k} = 1 + \left[\frac{(r_\eta)_{i,j,k}}{(r_\xi)_{i,j,k}}\right]^{0.5} + \left[\frac{(r_\zeta)_{i,j,k}}{(r_\xi)_{i,j,k}}\right]^{0.5}$$

where r_ξ, r_η and r_ζ are the scaled spectral radii of the convective flux Jacobian matrices (associated with the i, j and k directions).

The coefficients $\varepsilon^{(2i)}$ and $\varepsilon^{(4i)}$ are related to the pressure gradient parameter $v_{i,j,k}$ as follows:

$$\varepsilon^{(2i)} = \mu^{(2i)} \operatorname{Max}(v_{i,j,k}, v_{i+1,j,k})$$

$$v_{i,j,k} = \frac{|P_{i+1,j,k} - 2P_{i,j,k} + P_{i-1,j,k}|}{(1-\omega)(|P_{i+1,j,k} - P_{i,j,k}| + |P_{i,j,k} - P_{i-1,j,k}|) + \omega(P_{i+1,j,k} + 2P_{i,j,k} + P_{i-1,j,k})}$$

$$\varepsilon^{(4i)} = \operatorname{Max}(0, \mu^{(4i)} - \varepsilon^{(2i)})$$

where $\mu^{(2i)}$, $\mu^{(4i)}$ and ω are constants. The dissipation operators in the j and k directions are defined in a similar manner.

In the present study, the typical values of these parameters are taken as

$$\mu^{(2i)} = \mu^{(2j)} = \mu^{(2k)} = 0.2, \quad \mu^{(4i)} = \mu^{(4j)} = \mu^{(4k)} = 0.02, \text{ and } \omega = 0.35$$

5. NUMERICAL EXAMPLES

The basic accuracy of the current method has been tested for a number of applications. For all the computations, one order of magnitude drop in residual, that is to say, the accuracy level of 0.1, is used to control the subiterations at each time step for the pseudo-time marching. In the present study, it takes a few iterations (typically about five) to achieve the stopping criterion.

Unless stated, a nondimensional time step $\Delta t = 0.1$ is used for the steady flows, and $\Delta t = 0.05$ for the unsteady flows. The unsteady calculation usually takes 3–4 periods to get the solution fully periodic, when starting from its corresponding steady-state simulation.

All the structured grids are generated with an elliptic grid generation method that uses a forcing function control technique [21]. The distance of the first grid line off surface is about 10^{-5} characteristic length.

5.1. Examples of steady-state flows

5.1.1. Rear fuselage flow simulation at low Mach number. When the standard form of compressible Navier–Stokes equations, discretized with either centred or upwind schemes, are applied to some low speed steady flows by an explicit multi-stage Runge–Kutta method, two major effects on the solution are usually revealed, (1) a drastic slowdown of convergence rate, (2) an inaccurate or even incorrect solution.

The authors found that the stability, the convergence rate as well as the accuracy of the numerical process could be greatly enhanced in case the time-marching scheme was altered to an implicit one and no employment of the local time stepping.

In order to demonstrate the capabilities of the present method for low speed viscous problems, the flow about a general fuselage model has been simulated at a low Mach number of 0.2 and Reynolds number of 2.5 million. This model was designed to study the rear fuselage flow characteristics, and the measurement of pressure distributions was performed mainly on the rear part. The experimental results are only available for a minor part of the fuselage. Figure 1 shows the grid for this model. The grid number is $100 \times 51 \times 65 = 331\,500$.

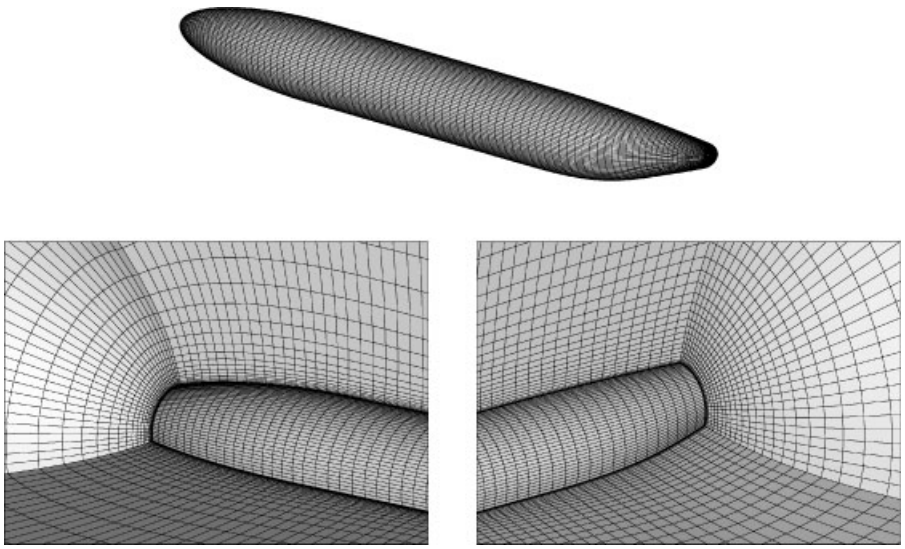

Figure 1. Grid for a general fuselage model.

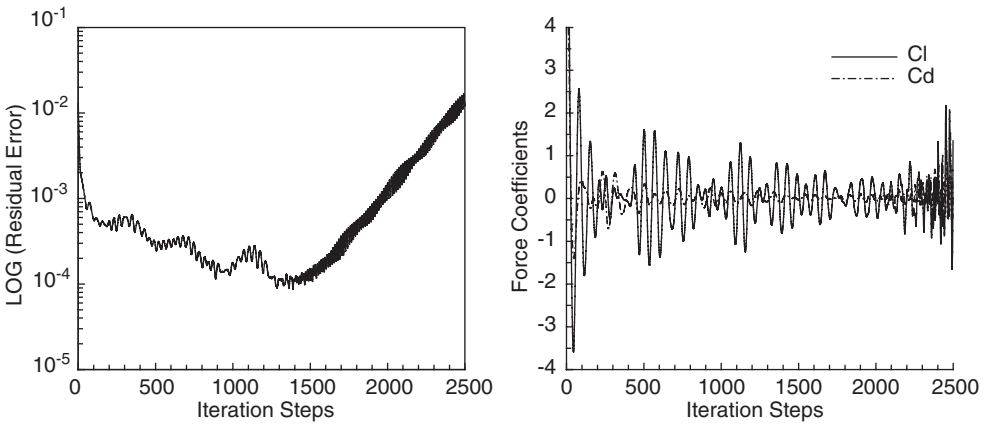

Figure 2. Convergence histories with an explicit Runge–Kutta code ($M = 0.2$, $\alpha = 4^\circ$).

With authors' computing practices, a successful Runge–Kutta code often failed to obtain a reliable convergent result, whereas the present fully implicit method resolved the numerical simulation of low speed flow over the single fuselage very well. Figure 2 shows the failed results from an explicit Runge–Kutta code that was well developed for transonic flows, even though the same grid and the same space discretization approach were employed for the Runge–Kutta method. Using the implicit code, the flow simulation needs about 2 h of CPU time for 300 time steps to converge on a personal computer Pentium IV 2.4G. Figure 3 shows

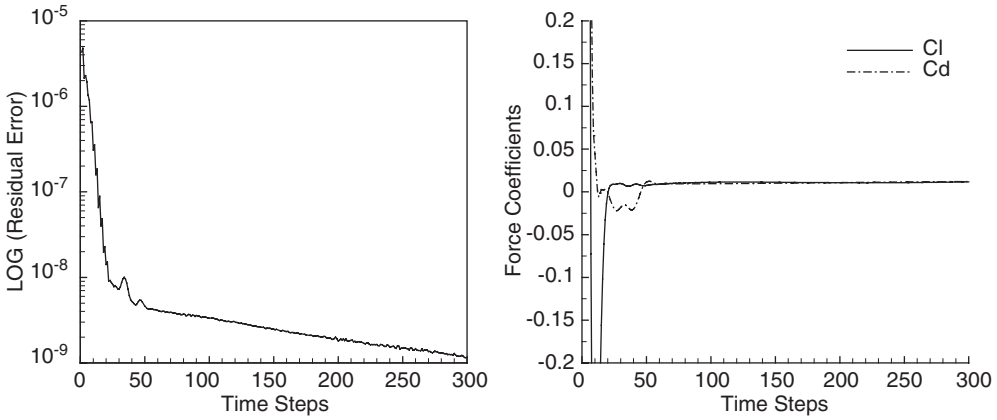

Figure 3. Convergence histories with the fully implicit method ($M = 0.2, \alpha = 4^\circ$).

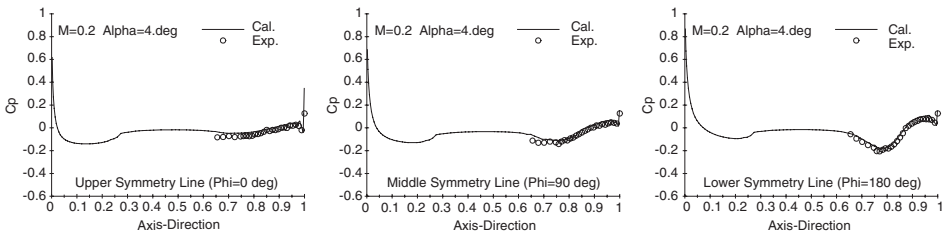

Figure 4. Streamwise pressure distributions along the fuselage model.

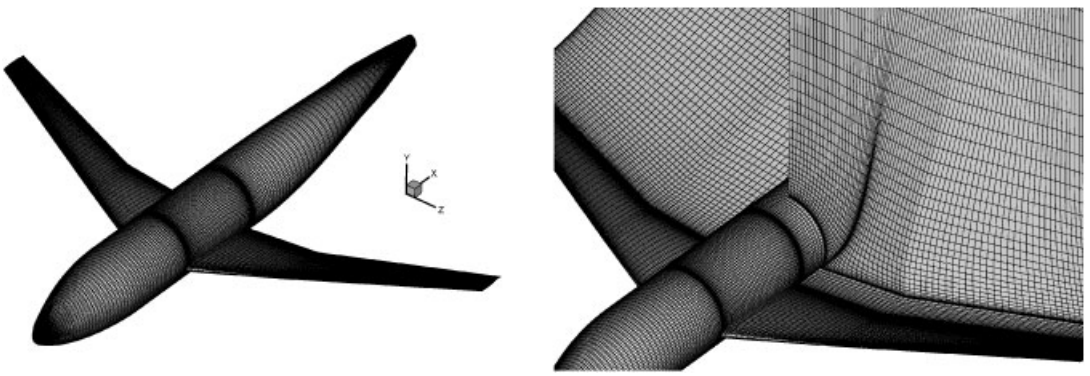

Figure 5. Grid system for DLR-F4 wing/body configuration.

the convergence histories for the residual and the computed aerodynamic force coefficients over iteration steps. In Figure 4 the computed pressure distributions are compared with the experimental data [22] along the upper, middle and lower lines on the fuselage.

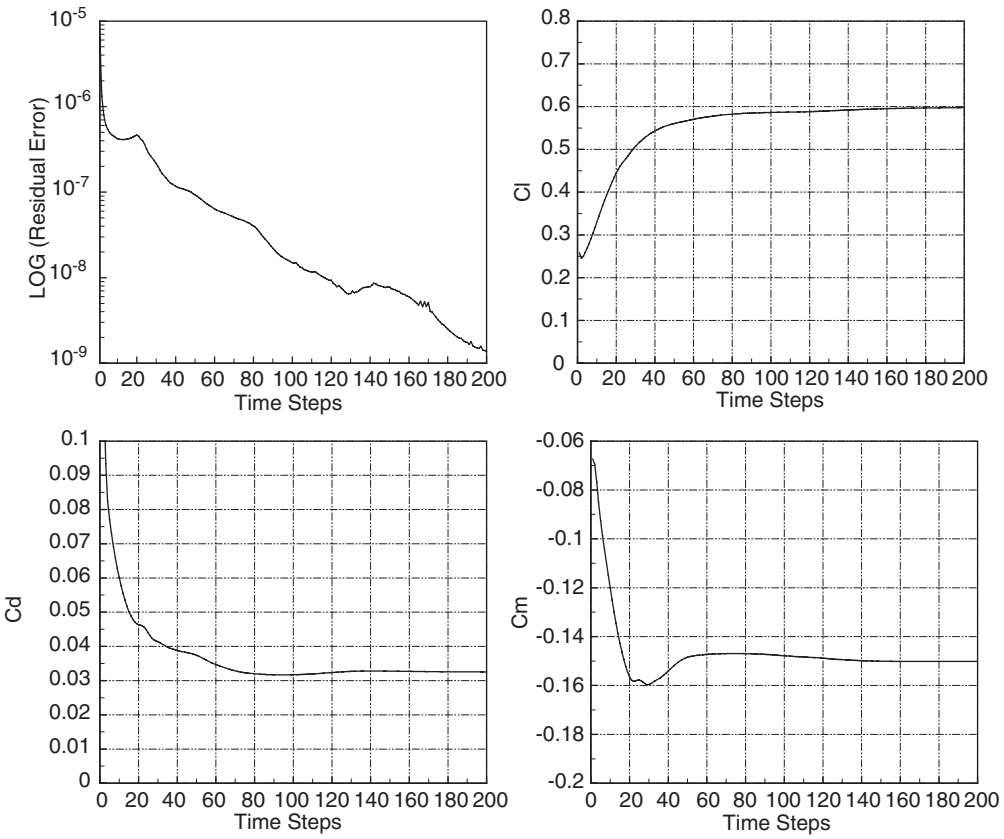

Figure 6. Convergence histories for DLR-F4 wing/body configuration ($C_L = 0.6$).

5.1.2. Transonic flow simulation for DLR-F4 wing/body configuration. To further verify the capability of the present method for steady viscous flows, a well-known and extensively studied configuration, DLR-F4 wing/body [23, 24], is used as a test case.

The grid system is shown in Figure 5. The total number of grid is $120 \times 65 \times 100 = 780\,000$. The flow condition selected for this analysis is $M_\infty = 0.75$, and the Reynolds number based on the aerodynamic mean chord length $Re = 3.0 \times 10^6$.

The numerical calculation is also performed on a Pentium IV computer. Figure 6 shows the corresponding convergence histories. It takes about 3 h of CPU time for 200 time steps to converge.

In Figure 7 the computed pressure distributions are compared with the experimental data [23] at selected spanwise stations for lift coefficients of 0.6. The computed force coefficients are compared with experimental results [23] in Table I. The computational results agree reasonably well with the experiment.

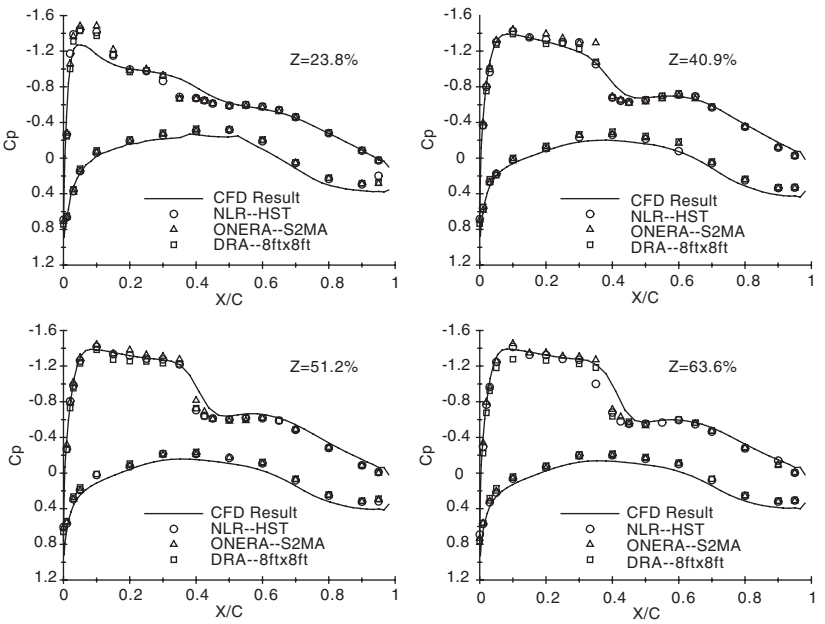

Figure 7. Comparison of computed and measured pressure distributions at selected wing sections for DLR-F4 wing/body configuration ($C_L = 0.6$).

Table I. Comparison of computed force coefficients with the experiment results.

	C_l	C_d	C_m
Cal.	0.5976	0.03254	−0.1501
NLR-HST [23]	0.583	0.033	−0.129
	0.624	0.036	−0.130
ONERA-S2MA [23]	0.609	0.035	−0.126
DRA-8ft × 8ft [23]	0.609	0.034	−0.136

5.2. *Examples of unsteady-state flows*

5.2.1. Unsteady transonic flow simulation over pitching LANN wing. The time-accuracy of the present method is validated for the oscillating LANN wing [25]. The LANN wing is typical for a transport type wing with a supercritical airfoil section, leading- and trailing-edge sweep and high aspect ratio. Figure 8 shows the surface and root sectional grids for this wing.

For this test case, all the unsteady flows performed pitching oscillations with a periodic motion defined by the angle of attack as a function of time given by

$$\alpha(t) = \alpha_m + \alpha_0 \sin(2kt)$$

where α_m is the mean model incidence, α_0 the oscillation amplitude and k the reduced frequency of the pitching motion.

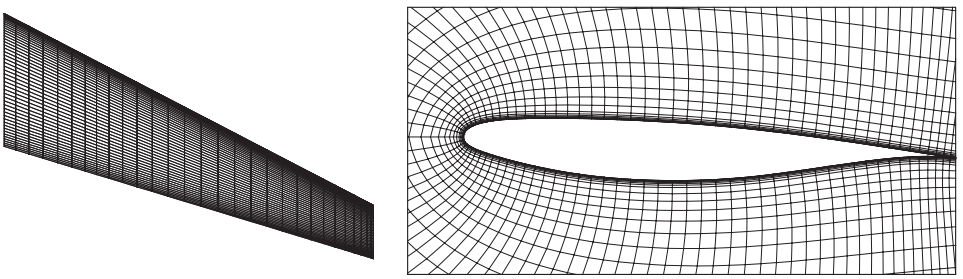

Figure 8. Surface and root sectional grids for LANN wing.

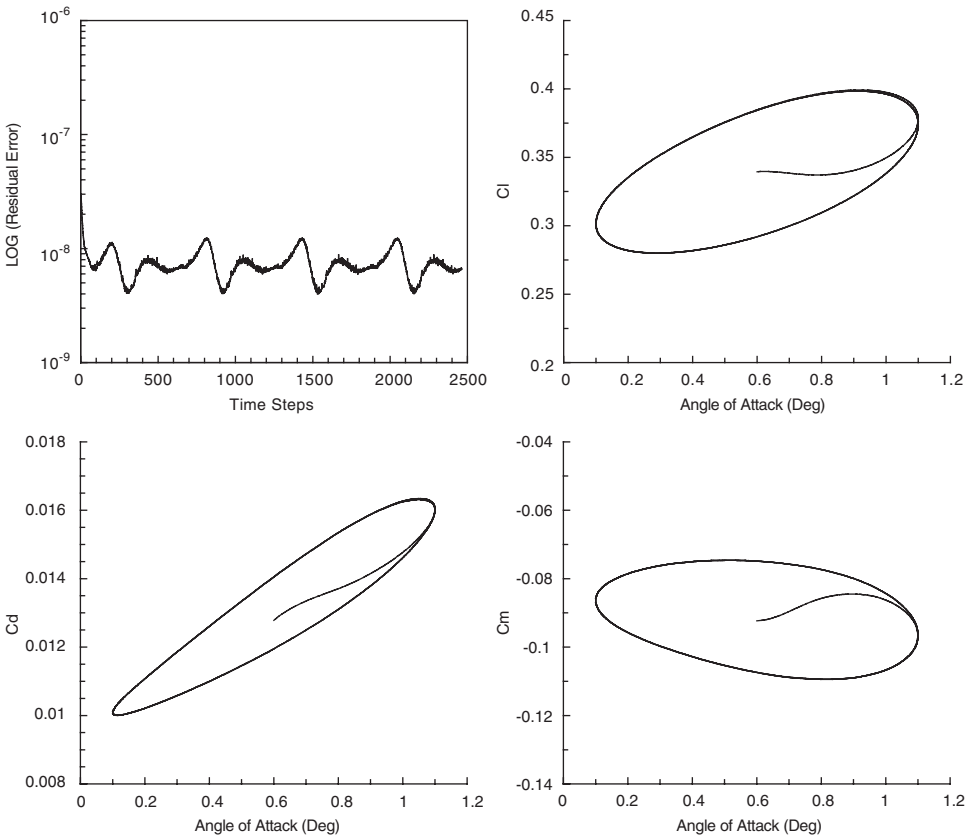

Figure 9. Convergence histories for LANN wing.

The presented results here refer to the selected flow condition, $M_\infty = 0.82$, $Re = 5.4 \times 10^6$, and $\alpha_m = 0.6°$, $\alpha_0 = 0.5°$, $k = 0.076$. Here the Reynolds number and the reduced frequency are based on the aerodynamic chord length. The wing pitches about an unswept axis at 62.1% of the root chord from the wing apex.

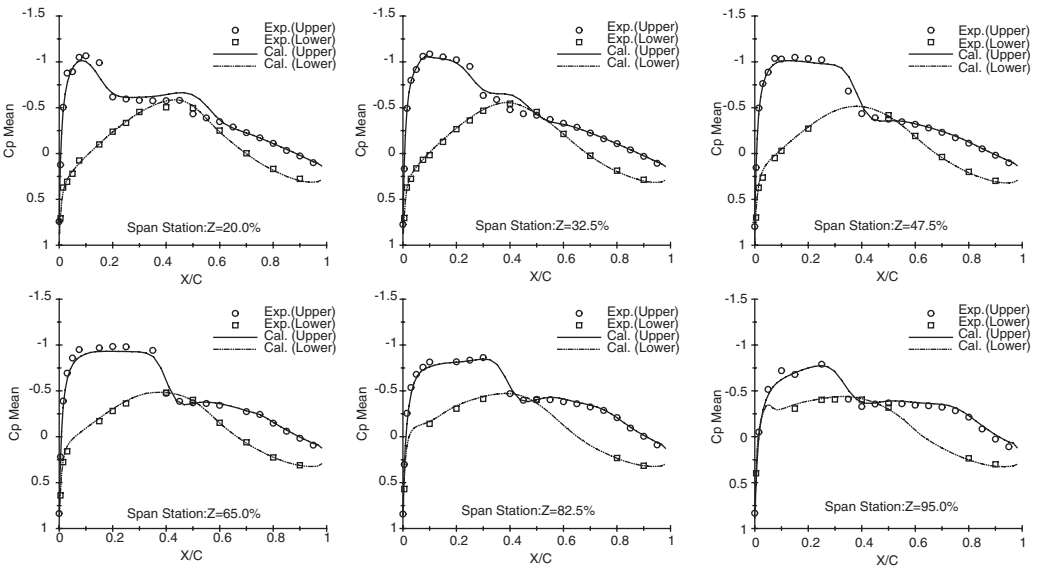

Figure 10. Spanwise comparison of mean pressure distributions for a rigidly pitching LANN-wing.

The grid used in the computation consists of $165 \times 50 \times 60 = 495\,000$ cells. The corresponding CPU time is about 6 h for one period on a personal computer Pentium IV 2.4G. The time histories of the residual error and the computed force coefficients vs. the iteration steps and the time dependent angle of attack are shown in Figure 9.

In Figure 10 the mean pressure distributions at six sections on the wing are compared with experiment [25]. Figures 11 and 12 show the unsteady pressures in real and imaginary parts as well as their comparisons with experimental data [25]. For this case, a good agreement of the computed results and experimental data is achieved in general. This indicates with the present dual-time stepping approach 3D viscous time-accurate simulations are feasible for unsteady flows.

5.2.2. Unsteady transonic flow simulation over pitching NACA 64A010 airfoil. For NACA 64A010 airfoil, the incidence as a function of time is given by

$$\alpha(t) = \alpha_m + \alpha_0 \cos(2kt)$$

The flow condition selected for this analysis is $M_\infty = 0.797$, $Re = 1.24 \times 10^7$, and $\alpha_m = -0.08°$, $\alpha_0 = 2.0°$, $k = 0.101$.

The grid number is $165 \times 2 \times 60 = 19\,800$. This is a 3D simulation of a 2D problem. Also on a Pentium IV computer, it only needs about 15 min for one period.

In this test case, the unsteady calculation is started from freestream condition. Figure 13 shows the time histories of the residual error and the computed force coefficients *vs* the iteration steps and the time dependent angle of attack are presented. In Figure 14 the computed results are compared with the experimental data that was given by Davis [25].

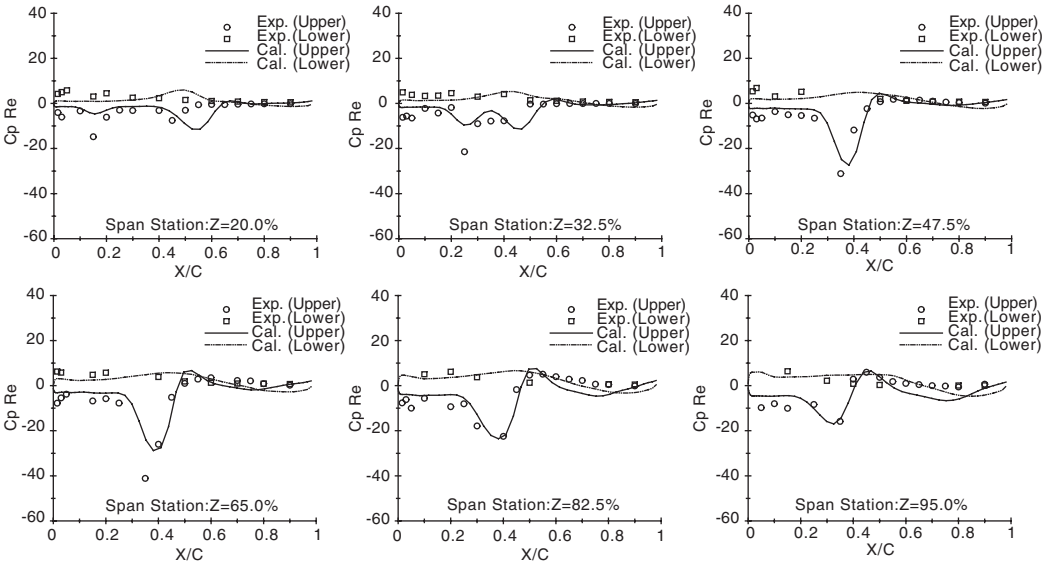

Figure 11. Spanwise comparison of unsteady pressure distributions in real part for a rigidly pitching LANN-wing.

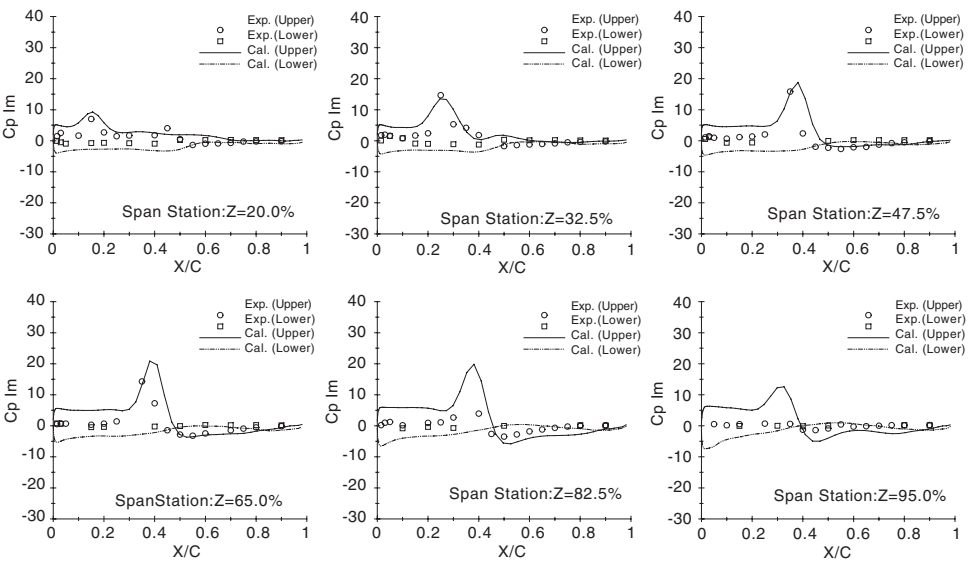

Figure 12. Spanwise comparison of unsteady pressure distributions in imaginary part for a rigidly pitching LANN-wing.

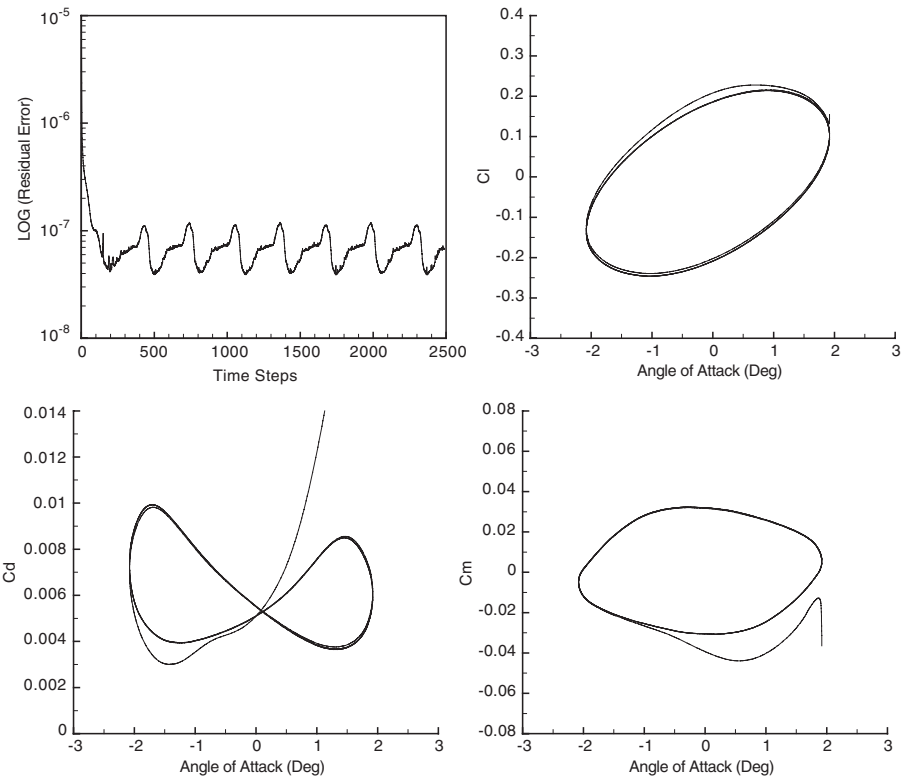

Figure 13. Convergence histories for NACA 64A010 airfoil.

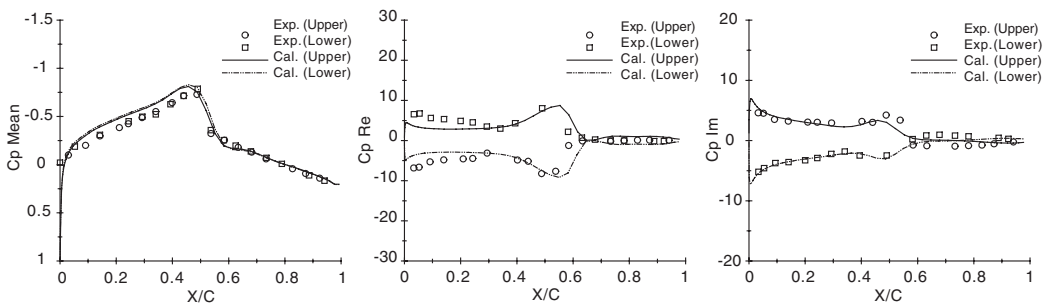

Figure 14. Comparison of computed pressure distribution with experiment for NACA 64A010 airfoil.

6. CONCLUSIONS AND OUTLOOK

A time-accurate, fully implicit method has been applied to solve a variety of steady and unsteady viscous flow problems on structured grids. With a dual-time approach proposed by Jameson, a Newton-like subiteration is implemented into the original LU-SGS method to

enhance the temporal accuracy of the numerical scheme. At convergence of the subiterations, a second-order time-accurate scheme is obtained. The numerical results obtained in this study indicate that the presently developed dual-time-marching strategy is an efficient option, which was proven to be very reliable, robust, and accurate for steady and unsteady viscous flow simulations, especially for some low speed flow problems.

In the present work, only the algebraic Baldwin–Lomax model is used, and it is assumed that the grid system is rigidly rotated with the wing in the case of unsteady flow simulations. Further studies of the approach are clearly needed. Future work involves the application of the two-equation turbulence model and the extension of the method for problems with deforming geometries.

ACKNOWLEDGEMENTS

This work was supported in part by the fund of 'The Developing Program for Outstanding Persons' at Northwestern Polytechnical University for the first author.

REFERENCES

1. Swanson RC, Turkel E. A multistage time-stepping scheme for the Navier–Stokes equations. *AIAA Paper* 85-0035, 1985.
2. Radespiel R, Swanson RC. An investigation of cell centered and cell vertex multigrid schemes for the Navier–Stokes equations. *AIAA Paper* 89-0548, January 1989.
3. Radespiel R, Rossow CC, Swanson RC. Efficient cell-vertex multigrid scheme for the three-dimensional Navier–Stokes equations. *AIAA Journal* 1990; **28**(8):1464–1472.
4. Rossow CC, Kroll N, Radespiel R, Scherr S. Investigation of the accuracy of finite volume methods for 2- and 3-dimensional flows. *AGARD-CP*-437 1988; **2**:17.1–17.11.
5. Jayaram M, Jameson A. Multigrid solution of the Navier–Stokes equations for flows over wings. *AIAA Paper* 88-0705, January 1988.
6. Kroll N, Radespiel R, Rossow CC. Accurate and efficient flow solvers for 3D applications on structured meshes. *AGARD Report* R-807, 1995; 4.1–4.59.
7. Grasso F, Marini M. LU implicit TVD scheme for the solution of viscous two dimensional high speed flows. *AIAA Paper* 91-1573-Cp, 1991.
8. Matsuno K. A time-accurate iterative scheme for solving the unsteady compressible flow equations. *AIAA Paper* 89-1992-Cp, 1989.
9. Shang JS, Scherr SJ. Navier–Stokes solution of the flow field around complete aircraft. *AIAA Paper* 85-1509, January 1985.
10. Yoon S, Jameson A. Lower-upper symmetric-Gauss–Seidel method for the Euler and Navier–Stokes equations. *AIAA Paper* 87-0600, 1987.
11. Rieger H, Jameson A. Solution of steady three dimensional compressible Euler and Navier–Stokes equations by an implicit LU scheme. *AIAA Paper* 88-0619, 1988.
12. Yoon S, Kwak D. Implicit Navier–Stokes solver for three dimensional compressible flow. *AIAA Journal* 1992; **30**(11):2653–2659.
13. Klopfer GH, Yoon S. Multizonal Navier–Stokes code with the LU-SGS scheme. *AIAA Paper* 93-2965, 1993.
14. Jameson A, Turkel E. Implicit schemes and LU decompositions. *Mathematics of Computation* 1981; **37**(156):385–397.
15. Buratynski EK, Caughey DA. An implicit LU scheme for the Euler equations applied to arbitrary cascades. *AIAA Journal* 1986; **24**(1):39–46.
16. Jameson A, Yoon S. Lower-upper implicit schemes with multiple grids for the Euler equations. *AIAA Journal* 1987; **25**(7):929–935.
17. Jameson A. Time dependent calculations using multigrid with applications to unsteady flows past airfoils and wings. *AIAA Paper* 91-1956, June 1991.
18. Baldwin BS, Lomax H. Thin layer approximation and algebraic model for separated turbulent flows. *AIAA Paper* 78-257, 1978.
19. Chaderjian NM, Numerical algorithm comparison for the accurate and efficient computation of high-incidence vortical flow. *AIAA Paper* 91-0175, January 1991.

20. Turkel E, Vatsa VN. Effect of artificial viscosity on three-dimensional flow solutions. *AIAA Journal* 1994; **32**(1).
21. Higenstock A. A fast method for the elliptic generation of three dimensional grids with full boundary control. *Numerical Grid Generation In Computational Fluid Mechanics* '88. Pineridge: Swansea, Wales, U.K., 1988; 137–146.
22. Zhang ZL, Liu JC. Low speed test results of flow characteristics about various rear fuselages. *Technical Report* of Xi'an Aircraft Design and Research Institute, May 2001.
23. Redeker G. DLR-F4 wing body configuration. In *A Selection of Experimental Test Cases for the Validation of CFD Codes*, AGARD-AR-303, vol. II. August 1994, Chapter B.
24. Redeker G, Mueller R, Ashill PR, Elsenaar A, Schmitt V. Experiments on the DFVLR-F4 wing body configuration in several European wind tunnels. *AGARD-CP*-429, July 1988.
25. Davis H. Compendium of unsteady aerodynamic measurements. *AGARD Report No*. 702, 1983.

